Available online at www.sciencedirect.com
SCIENCE DIRECT®
Journal of Solid State Chemistry 171 (2003) 7–11
JOURNAL OF SOLID STATE CHEMISTRY
http://elsevier.com/locate/jssc

Cerium oxide for sunscreen cosmetics

Shinryo Yabe[a,*] and Tsugio Sato[b]

[a] Research and Development Division, KOSÉ Corporation, 48-18 Sakae-cho, Kita-ku, Tokyo 114-0005, Japan
[b] Institute of Multidisciplinary Research for Advanced Materials, Tohoku University, 2-1-1 Katahira, Aoba-ku, Sendai 980-8577, Japan

Received 17 April 2002; received in revised form 1 August 2002; accepted 11 November 2002

Abstract

Ultrafine particles of M^{n+}-doped ceria ($M^{n+} = Mg^{2+}$, Ca^{2+}, Sr^{2+}, Ba^{2+}, Y^{3+}, La^{3+}, Nd^{3+}, Sm^{3+}, Eu^{3+}, Tb^{3+}) for UV filter were prepared via soft solution chemical routes at 40°C. X-ray diffraction revealed that the prepared doped particles had the cubic fluorite structures although peak positions changed depending on the kind and amount of doped metal ion. Doping with 20 mol% Ca^{2+} and 20 mol% Zn^{2+} resulted in extremely decreasing the particle size (2–4 nm) and the catalytic activity of ceria for oxidation of castor oil. Ca^{2+}-doped cerium dioxide showed excellent UV absorbing effect and transparency in the visible ray region compared with undoped cerium dioxide.

Keywords: Doped ceria; Ca^{2+}; Zn^{2+}; Ultrafine particle; UV filter; Catalytic activity

1. Introduction

Ultrafine ceria (CeO_2) has characteristics ideal for use as a broad-spectrum inorganic sunscreen in personal-care products: it is relatively transparent to visible light, but has excellent ultraviolet radiation absorption properties, and appears natural on the skin without imparting an excessively pale-white look. Many studies have reported the synthesis of nano-sized particles of ceria with various purposes [1–7]. However, because of its high catalytic activity for the oxidation of organic materials, ceria has seldom been used commercially as a sunscreen material. Ultrafine titania and zinc oxide are effective inorganic sunscreens widely used for this purpose. Their high refractive indices, however, can make the skin look unnaturally white when incorporated into the products. In addition, their high photocatalytic activity facilitates the generation of reactive oxygen species [8], which can oxidize and degrade other ingredients in the formulation, raising safety concerns. The goal of the present study was to find a way to overcome this problem and to develop a safe, stable inorganic sunscreen with superior UV absorption capability. In a previous study [9], we reported that the catalytic activity of ceria could be successfully decreased by coating with amorphous silica. This material has been used in cosmetic formulations; however, coating with amorphous silica resulted in a decrease of the UV-shielding effect. By doping CeO_2 with a metal ion possessing lower valence and/or larger ionic size than those of Ce^{4+}, we succeeded in synthesizing novel nanoparticles with significantly reduced oxidation catalytic activity.

2. Experimental

2.1. Chemicals

All chemicals were of reagent grade and used without further purification.

2.2. Preparation of doped ceria

Ultrafine particles of M^{n+}-doped ceria were prepared via soft solution chemical routes at 40°C as follows. At first, 0.8 M $CeCl_3$ and 0.2 M MCl_n mixed aqueous solution ($M^{n+} = Mg^{2+}$, Ca^{2+}, Sr^{2+}, Ba^{2+}, Y^{3+}, La^{3+}, Nd^{3+}, Sm^{3+}, Eu^{3+}, Tb^{3+}) and 3 M NaOH aqueous solution were simultaneously dropped into distilled water at 40°C with stirring to precipitate M^{n+}-doped $Ce(OH)_3$. Then H_2O_2 aqueous solution was added to

*Corresponding author. Fax: +81-3-3919-0734.
E-mail address: sh-yabe@kose.co.jp (S. Yabe).

0022-4596/03/$ - see front matter © 2003 Elsevier Science (USA). All rights reserved.
doi:10.1016/S0022-4596(02)00139-1

oxidize M^{n+}-doped $Ce(OH)_3$ to form M^{n+}-doped CeO_2. When needed, the solution pH was adjusted with 1 M NaOH and/or 1 M HCl. Finally, the precipitates were washed with water and methyl alcohol and dried at 120°C.

2.3. Analysis

The precipitate morphology was examined using a transmission electron microscope (TEM, JEOL, JEM-1200EX2, JEM-3010, JEM-ARM1250). The crystalline phase identification was performed by the X-ray diffraction (XRD, Shimadzu, XD-01) method using graphite monochromatized Cu$K\alpha$ radiation. The specific surface area of the powders was measured by a conventional (BET) nitrogen adsorption method (Okura-riken, AMS-8000). The catalytic activity for the oxidation of organic material was determined by the conductometric determination method (Rancimat System) [10–12]. The sample powder (1 g) was mixed with castor oil (10 g) and set at 120°C with bubbling 0.5 L/min of air, where the air was introduced into distilled water attached to the electric conductivity measurement cell. The catalytic activity was evaluated by measuring the increase in the conductivity of distilled water by trapping volatile molecules formed by the oxidation of castor oil on heating. The photocatalytic activity was evaluated by measuring the degree of decomposition of phenol by irradiating a 100 W high-pressure mercury arc ($\lambda > 290$ nm) to 0.5 mM phenol solution containing 0.25 g of sample powder at 60°C with bubbling 100 mL/min of air. The UV-shielding properties of the particles were evaluated by measuring the transmittance of the film with uniformly dispersed sample powder using a UV–Vis spectrophotometer (Shimadzu, UV-2500PC), and 2 g of sample powder, 4 g of nitrocellulose of industrial grade, 10 g of ethyl acetate and 9 g of butyl acetate were mixed uniformly using paint shaker (Asada) and 100 g of zirconia ball, 2.7 mm in diameter, for 24 h. The dispersion mixture was applied onto a quartz glass plate with an applicator. The thickness of the film was 0.003 mm after drying at room temperature for 24 h.

3. Results and discussion

The high-resolution TEM micrographs suggested that the wet precipitate of $Ce(OH)_3$ consisted of rod-like particles (ca. 5 nm in diameter and 20 nm in length) which were composed of smaller rod-like particles (ca. 2 nm in diameter and 4 nm in length) as shown in Fig. 1. It is notable that rod-like and spherical particles of ceria were formed depending on the solution pH during the oxidation reactions of Ce(III) to Ce(IV). Namely, by adjusting the solution pH above 8 during both the neutralization reaction and oxidation reaction, ceria powder, which consisted of rod-like particles similar to $Ce(OH)_3$ particles were formed as shown in Fig. 2. However, the ceria particles formed by adjusting the solution pH above 8 and below 7 during the neutralization reaction and oxidation reaction, respectively, were spherical as shown in Fig. 3. Matijevic [13–15] has pointed out that the formation of spherical CeO_2 particles of narrow size distributions, consisting of a large number of small subunits, is caused by the uniformity of the latter and the chemical surface reactions taking place on their collisions. He also showed that the CeO_2 dispersions of hexagonal particles consisted of solids with spherical-shaped subunits. This suggests that the formation of large rod-like CeO_2 particles consisting of small subunits of rod-like CeO_2 particles were prepared in solutions with a pH above 8 during both the neutralization and oxidation reactions. In solutions below pH 7 during the oxidation reaction, we observed, with the TEM, that the rod-like $Ce(OH)_3$

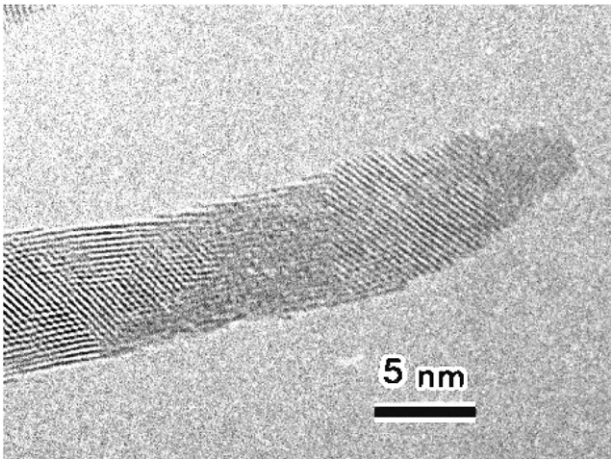

Fig. 1. TEM micrograph of $Ce(OH)_3$.

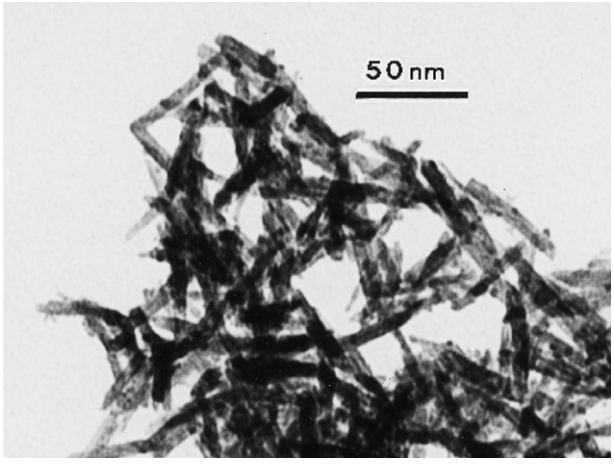

Fig. 2. TEM micrograph of the ceria particles formed by adjusting the solution pH above 8 during both the neutralization and oxidation reactions.

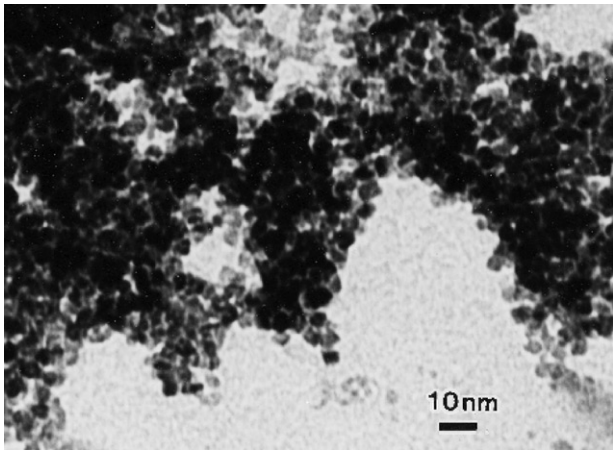

Fig. 3. TEM micrograph of the ceria particles formed by adjusting the solution pH above 8 and below 7 during the neutralization and oxidation reactions, respectively.

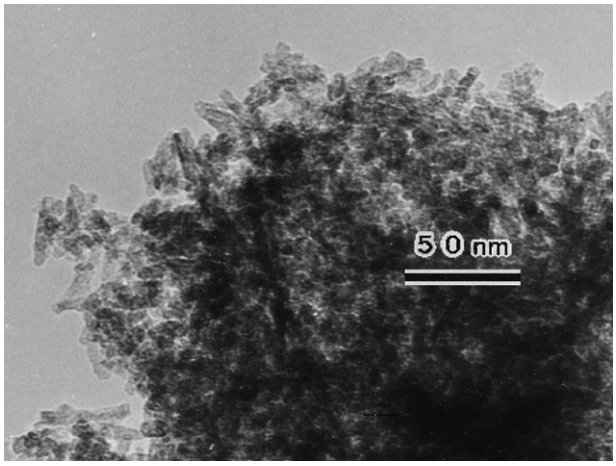

Fig. 4. TEM micrograph of 20 mol% Ca^{2+}-doped ceria particles formed by adjusting the solution pH above 8 during both the neutralization and oxidation reactions.

particles had begun to separate into spherical-shaped subunits after a few minutes to form spherical CeO_2. Therefore, the oxidation reaction appeared to proceed by a topotactic reaction mechanism and a dissolution–precipitation mechanism in alkaline solution and acidic solution, respectively.

Furthermore, spherical ceria particles were also obtained by conducting a neutralization reaction and an oxidation reaction simultaneously. A $CeCl_3$ and MCl_2 mixed aqueous solution and NaOH aqueous solution, were combined to initiate the neutralization reaction. As the neutralization reaction proceeded, the presence of H_2O_2, which had also been added, allowed spontaneous oxidation of $Ce(OH)_3$ particles in the oxidation reaction. This reaction was not dependent on the pH value. It may be due to the lack of time to grow rod-like $Ce(OH)_3$ particles since the $Ce(OH)_3$ particles formed should be immediately oxidized to ceria under such reaction conditions. The particle size of ceria also greatly changed depending on the kind of doped metal ion. Doping 20 mol% Ca^{2+} with ceria prepared by adjusting the solution to above pH 8 during both the neutralization reaction and oxidation reaction resulted in decreasing particle size to 2–4 nm, whereas doping 30 mol% Eu^{3+} slightly increased the particle size as shown in Figs. 4 and 5, respectively. By doping 20 mol% Zn^{2+} with ceria, the particle size also decreased, but the shape of the particles was spherical at all oxidation pH conditions.

BET specific surface areas of undoped ceria and 20 mol% Ca^{2+}-doped ceria were 67 and 111 m^2/g, respectively. The peak position of X-ray diffraction of ceria slightly shifted depending on the kind and amount of dopant. Figure 6 shows the lattice constant of Ca^{2+}- and Zn^{2+}-doped ceria.

The catalytic activity for the air oxidation of castor oil at 120°C decreased substantially by doping with Ca^{2+}

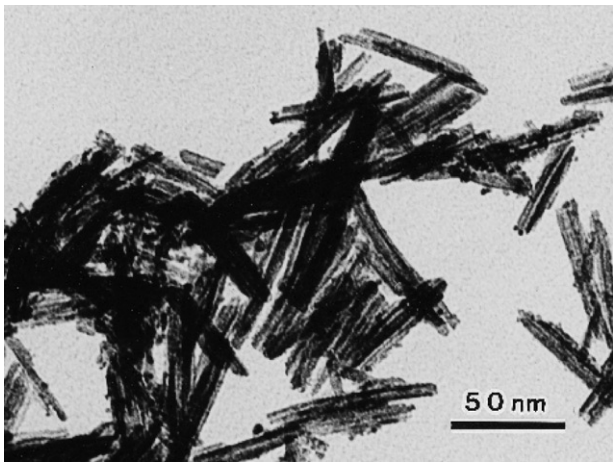

Fig. 5. TEM micrograph of 30 mol% Eu^{3+}-doped ceria particles formed by adjusting the solution pH above 8 during both the neutralization and oxidation reactions.

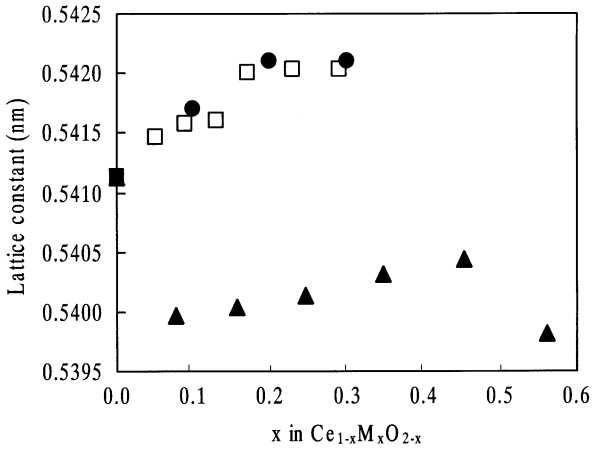

Fig. 6. Lattice constant of Ca^{2+}- and Zn^{2+}-doped ceria samples treated at 1000°C. ●: Ca^{2+}-doped ceria, □: Ca^{2+}-doped ceria [16] and ▲: Zn^{2+}-doped ceria.

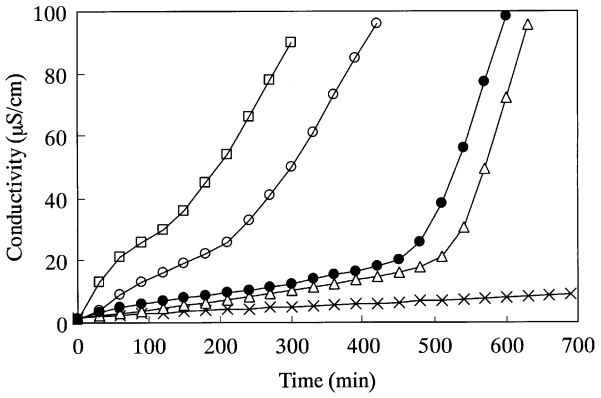

Fig. 7. Evaluation of the catalytic activity at 120°C using the Rancimat System. ×: blank (without catalyst), □: undoped CeO_2, △: 20 mol% Ca^{2+}-doped CeO_2, ●: 20 mol% Zn^{2+}-doped CeO_2 and ○: 30 mol% Eu^{3+}-doped CeO_2.

and Zn^{2+} (Fig. 7). Doping 10 mol% Nd^{3+}, 10 mol% Sm^{3+} and 30 mol% Eu^{3+} also resulted in a decrease in the catalytic activity for oxidation, but the decrease was not so much as in case of doping Ca^{2+}. From these findings, the effect of the dopant was considered as follows; the catalytic activity of ceria must have been related to the oxygen evolution and absorption equilibrium reaction shown by

$$CeO_2 \rightleftarrows Ce^{4+}_{1-X}Ce^{3+}_{X}O_{2-X/2}\square_{X/2} + X/4O_2$$
$$\square:\ \text{Oxygen defect},\quad 0<X<1. \qquad (1)$$

The ideal $r(M^{n+})/r(O^{2-})$ ionic size ratio of MO_8 eight-coordination oxide is 0.732. In the case of the fluorite structure of ceria, $r(Ce^{4+})/r(O^{2+})$ is 0.703, which is smaller than that of the ideal value, indicating that Ce^{4+} is not large enough to stabilize the fluorite structure. To take on a more stable eight coordination of the fluorite structure, some Ce^{4+} would have a tendency to be reduced to Ce^{3+}, which has a larger ionic radius than Ce^{4+} as shown by Eq. (1). Accompanying this reaction, oxygen molecules are released to form oxygen vacancies. By doping Ca^{2+}, which possesses a lower valence and larger ionic size than Ce^{4+}, with CeO_2, we succeeded in stabilizing the fluorite structure of ceria and consequently reducing the oxidation catalytic activity.

However, it was confirmed that Zn^{2+} completely precipitated to form a solid solution with CeO_2. Since Zn^{2+} possesses smaller ionic size than Ce^{4+}, the low oxidation catalytic activity of Zn^{2+}-doped CeO_2 is suspected to be mainly due to the formation of the oxygen defect in CeO_2. The difference in the oxidation catalytic activity between Ca^{2+}- and Zn^{2+}-doped CeO_2 may be attributed to the difference in the ionic size of Ca^{2+} and Zn^{2+}.

Figure 8 shows the photocatalytic activity of ceria and titania where the surface areas of undoped ceria (Tokyo-Kasei), 20 mol% Ca^{2+}-doped CeO_2, and titania (Degussa P-25) were 9.3, 111 and 50 m^2/g, respectively.

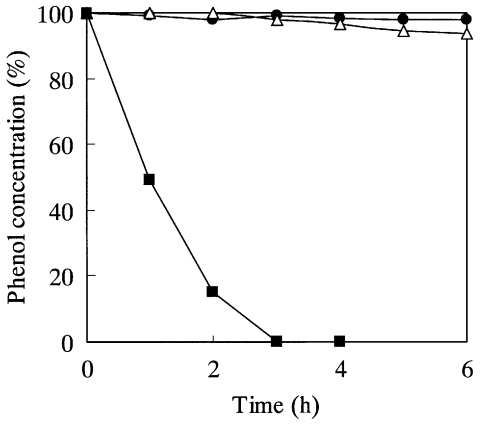

Fig. 8. Photocatalytic activity for the decomposition of phenol by irradiating UV ray ($\lambda > 290$ nm). △: commercial undoped CeO_2, ●: 20 mol% Ca^{2+}-doped CeO_2 and ■: TiO_2.

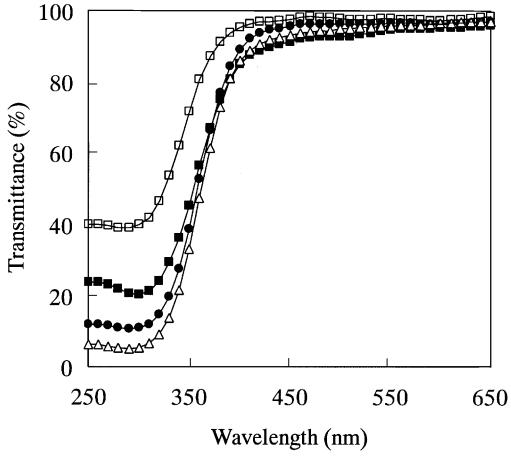

Fig. 9. UV–Vis transmittance spectra of thin films with undoped and doped CeO_2. ■: undoped ceria, ◆: 20 mol% Ca^{2+}-doped CeO_2, △: 20 mol% Zn^{2+}-doped CeO_2 and □: 30 mol% Eu^{3+} doped CeO_2.

The photocatalytic activity of both doped and undoped ceria was found to be much smaller than that of titania that perfectly decomposed phenol within 4 h. The low photocatalytic activity of ceria may be due to the existence of an oxygen defect formed by reaction (1), since it is known that the oxygen defect plays an important role to enhance the recombination reaction of photoinduced electrons and holes. Even undoped CeO_2 itself has a tendency to form an oxygen defect; by doping Ca^{2+} with CeO_2, formation of a greater oxygen defect and decreasing the photocatalytic activity of CeO_2 are expected. In the present study, there was little difference in the photocatalytic activities between undoped and doped CeO_2, and this may be attributed to the markedly lower photocatalytic activities of ceria, and even though there was a significant difference in the surface area, it was difficult to detect the difference under the present experimental conditions.

Figure 9 shows the UV–Vis transmittance spectra of undoped ceria, Ca^{2+}-, Zn^{2+}- and Eu^{3+}-doped ceria. Nanoparticles of 20 mol% Ca^{2+}-doped ceria resulted in an excellent UV-absorption capacity and high transparency in visible light compared with undoped ceria. These findings appeared to depend on the particle size and the aggregation condition of the particles, i.e., nanoparticles of Ca^{2+}-doped ceria might result in the formation of a dense film to increase the UV light absorption and decrease the scattering of the light to increase the transmittance of visible light. Doping 20 mol% Zn^{2+} resulted in an excellent UV-absorption capacity but the transparency in the visible light regions was inadequate. The value of the refractive index of CeO_2 ($n = 2.05$) is lower than the value of TiO_2 (Rutile) ($n = 2.72$), TiO_2 (anatase) ($n = 2.5$) and ZnO ($n = 2.2$). The decrease in the transparency may be attributed to the higher refractive index of ZnO.

UV filters used in personal care products must be safe for humans, and it is also required that they show both a high opacity in the UV region and high transparency in the visible spectrum. Nanosized 20 mol% Ca^{2+}- and Zn^{2+}-doped CeO_2 particles meet these criteria. The findings of the present study [17–19] revealed that nanoparticles of Ca^{2+}- and Zn^{2+}-doped CeO_2 can be safely used to provide a high sun protection factor (SPF) while maintaining a natural appearance when they are applied to the skin of humans.

4. Conclusions

Nanoparticles of M^{2+}-doped ceria were prepared via soft solution chemical routes. Doping 20 mol% Ca^{2+} and 20 mol% Zn^{2+} with ceria substantially decreased the catalytic activity for the air oxidation of castor oil. There was a clear advantage with 20 mol% Ca^{2+}- and Zn^{2+}-doped CeO_2 as an inorganic UV filter because of its excellent UV-absorption capacity, high transparency in visible light and low oxidation and photocatalytic activity.

References

[1] D.I. Ryabchikov, V.A. Ryuabukin, in: A. Arbor (Ed.), Analytical Chemistry of Yttrium and the Lanthanide Elements, Ann Arbor-Humphrey Science, Michigan, 1970, p. 50 (Chapter 3).
[2] P. Chen, I. Chen, J. Am. Ceram. Soc. 76 (1993) 1577.
[3] Y. Zhou, R. Phillips, J. Switzer, J. Am. Ceram. Soc. 78 (1995) 981.
[4] M. Hirano, E. Kato, J. Am. Ceram. Soc. 79 (1996) 777.
[5] T. Masui, K. Fujiwara, K. Machida, T. Sakata, H. Mori, G. Adachi, Chem. Mater. 9 (1997) 2197.
[6] T. Masui, K. Machida, T. Sakata, H. Mori, G. Adachi, J. Alloys Compds. (1997) 127.
[7] X. Yu, F. Li, X. Ye, X. Xin, Z. Xue, J. Am. Ceram. Soc. 83 (2000) 964.
[8] R. Cai, K. Hashimoto, K. Ito, Y. Kubota, A. Fujishima, Bull. Chem. Soc. Jpn. 64 (1991) 1268.
[9] S. Yabe, S. Momose, J. Soc. Cosmet. Chem. Jpn. 32 (1998) 372.
[10] J. Frank, J.V. Geil, R. Freaso, Food Technol. 6 (1982) 71.
[11] M.W. Laubli, P.A. Bruttel, J. Am. Oil Chem. Soc. 63 (1986) 792.
[12] C. Kato, et al., J. Jpn. Oil Chem. Soc. 42 (1993) 55–61.
[13] W.P. Hsu, L. Ronnquist, E. Matijevic, Langmuir 4 (1988) 31.
[14] E. Matijevic, Langmuir 10 (1994) 8.
[15] E. Matijevic, W.P. Hsu, J. Colloid Interface Sci. 118 (1987) 506.
[16] W. Huang, P. Shuk, M. Greenblatt, Chem. Mater. 9 (1997) 2240.
[17] S. Yabe, M. Yamashita, S. Momose, K. Tahira, S. Yoshida, R. Li, S. Yin, T. Sato, Int. J. Inorg. Mater. 3 (2001) 1003–1008.
[18] M. Yamashita, K. Kameyama, S. Yabe, S. Yoshida, Y. Fujishiro, T. Kawai, T. Sato, J. Mater. Sci. 37 (2002) 683–687.
[19] R. Li, S. Yabe, M. Yamashita, S. Momose, S. Yoshida, S. Yin, T. Sato, Mater. Chem. Phys. 75 (2002) 39–44.